Search for CP Violation in Ξ and Λ Hyperon Decays with the HyperCP Spectrometer at Fermilab

C. Materniak[a*]

[a]Department of Physics, University of Virginia
P.O. Box 400714, Charlottesville, VA 22904, USA

The HyperCP Collaboration at Fermilab is searching for *CP* violation in charged hyperon decays by comparing the angular decay distributions of protons and antiprotons from $\Xi^- \to \Lambda\pi^-$, $\Lambda \to p\pi^-$ and $\overline{\Xi}^+ \to \overline{\Lambda}\pi^+$, $\overline{\Lambda} \to \overline{p}\pi^+$ decays. Using a hyperon data sample orders of magnitude larger than any other experiment has collected, we report a preliminary result $A_{\Xi\Lambda} = [-6.0 \pm 2.1(\text{stat}) \pm 2.0(\text{syst})] \times 10^{-4}$, from an analysis of the entire HyperCP data set of over one billion events.

1. Introduction

First observed over forty years ago in K_L decays [1], charge-parity (*CP*) violation remains an interesting and mysterious topic in particle physics. As a necessary ingredient for explaining the prevalence of matter over antimatter in our universe [2], a comprehensive study of *CP* violation is of utmost importance. While the standard model allows for *CP* violation in weak interactions [3], the amount is too small [4] to account for the observed matter dominance. Observations of *CP* violation in neutral K [1] and B [5] decays have been largely consistent with the standard model, but some [6] may reflect contributions from new physics. The decays of hyperons are of particular interest as they are sensitive to beyond-the-standard-model sources of *CP* violation which kaons are not [7,8].

The decays of spin-$\frac{1}{2}$ hyperons proceed through parity-violating (S-wave) and conserving (P-wave) amplitudes. This manifests itself in the two-body non-leptonic weak decays such that the daughter baryon has an anisotropic decay distribution given by

$$\frac{dN}{d\Omega} = \frac{N_0}{4\pi}(1 + \alpha\vec{P}_p \cdot \hat{p}_d), \tag{1}$$

where $\vec{P}_p$ is the parent hyperon polarization, $\hat{p}_d$ is the daughter baryon momentum unit vector, and $\alpha = 2\text{Re}(S^*P)/(|S|^2 + |P|^2)$. The magnitude of the parity violation is given by the decay-dependent α parameter; *CP* invariance requires that $\alpha = \overline{\alpha}$ [9].

In HyperCP, Ξ^- and $\overline{\Xi}^+$'s were produced at 0° ensuring, by parity invariance in strong interactions, that their polarization was zero. A charged Ξ decays into a Λ and a π 99% of the time. When the parent Ξ's are unpolarized, the Λ is produced in a helicity state with polarization $\vec{P}_\Lambda = \alpha_\Xi \hat{p}_\Lambda$ [10]. Combining this with Eq. 1 the angular distribution of p's from unpolarized $\Xi^- \to \Lambda\pi^- \to p\pi^-\pi^-$ decays is then given by

$$\frac{dN}{d\cos\theta} = \frac{N_0}{2}(1 + \alpha_\Xi\alpha_\Lambda\cos\theta). \tag{2}$$

The polar angle θ is measured in the Λ helicity frame in which the direction of the Λ in the Ξ^- rest frame defines the polar axis. If *CP* is conserved the angular distribution of $\overline{p}$'s from the corresponding decay sequence, $\overline{\Xi}^+ \to \overline{\Lambda}\pi^+ \to p\pi^+\pi^+$ is identical as both α_Ξ and α_Λ reverse sign under *CP*. Any difference in these angular distributions is evidence of *CP* violation in either the Ξ or Λ decays, or possibly both. The *CP*-violating observable is

$$A_{\Xi\Lambda} \equiv \frac{\alpha_\Xi\alpha_\Lambda - \overline{\alpha}_\Xi\overline{\alpha}_\Lambda}{\alpha_\Xi\alpha_\Lambda + \overline{\alpha}_\Xi\overline{\alpha}_\Lambda} \approx A_\Xi + A_\Lambda, \tag{3}$$

where

$$A_\Xi \equiv (\alpha_\Xi + \overline{\alpha}_\Xi)/(\alpha_\Xi - \overline{\alpha}_\Xi), \tag{4}$$

*Representing the HyperCP Collaboration.

and

$$A_\Lambda \equiv (\alpha_\Lambda + \overline{\alpha}_\Lambda)/(\alpha_\Lambda - \overline{\alpha}_\Lambda). \quad (5)$$

2. Theoretical Predictions and Previous Measurements

Standard model predictions for the combined asymmetry have fallen steadily since early calculations [11]. The most recent calculation from chiral perturbation theory puts the asymmetry between $-0.5 \times 10^{-4} \leq A_{\Xi\Lambda} \leq 0.5 \times 10^{-4}$ [12], too small to detect with the HyperCP data. Note that this prediction uses a theoretical calculation of the S- and P-wave $\Lambda\pi$ final-state scattering phase-shift differences [13] rather than more recent measurements [14]. While the standard-model predictions of the *CP* asymmetry are small, calculations from left-right symmetric [11] and supersymmetric models [15,16], allow for larger *CP* asymmetries. The supersymmetric calculation of He *et al.* generates values of A_Λ as large as 19×10^{-4} [15]. Bounds from ϵ and ϵ'/ϵ measurements in neutral K decays, limit $A_{\Xi\Lambda}$ to be less than 97×10^{-4} [8].

Experiments prior to HyperCP have only managed to probe hyperon *CP* asymmetries at the $O(10^{-2})$ level. The best pre-HyperCP measurement came from E756 at Fermilab which found $A_{\Xi\Lambda}$ to be 0.012 ± 0.014 [17]. In 2004, the HyperCP collaboration published a result 20 times more precise, $A_{\Xi\Lambda} = [0.0 \pm 5.1(\text{stat}) \pm 4.4(\text{syst})] \times 10^{-4}$ [18], using 17% of the data sample. In this paper we present a preliminary result for the measurement of $A_{\Xi\Lambda}$ from the full HyperCP datset.

3. Experimental Apparatus

Data were taken at Fermilab using a high-rate spectrometer (Fig. 1) specifically designed for measuring *CP* violation in hyperon decays [19]. Hyperons were produced via 800 GeV/c incident protons on a Cu target measuring $2 \times 2\,\text{mm}^2$ in cross section. Following the target was a 6.096 m long dipole magnet ("Hyperon Magnet") with an embedded curved collimator that selected Ξ's with an average momentum of 157 GeV/c. Following the Hyperon Magnet the particles traveled through a 13 m long evacuated pipe in which most of the Ξ and Λ's decayed. Multiwire proportional chambers (MWPCs) were placed upstream and downstream of a pair of dipole magnets ("Analyzing Magnets") for measuring the momenta of the Ξ and Λ daughter particles. Triggering was done using two scintillator hodoscopes and a fast hadronic calorimeter near the rear of the spectrometer. The opposite-sign (OS) and same-sign (SS) hodoscopes were placed to beam-left and beam-right of the secondary beam respectively, and the calorimeter was placed behind the OS hodoscope. For rare decay searches, two muon stations composed of three layers of iron absorber followed by proportional tubes were positioned at the end of both spectrometer arms.

Switching from Ξ^- (negative) to $\overline{\Xi}^+$ (positive) running modes was done by simply reversing the polarity of the Hyperon and Analyzing Magnets. In order to match the secondary-beam rates, differing target lengths were used for each mode of operation. Negative and positive data were taken alternately, typically in a sequence of three positive runs followed by one negative run. At a nominal primary proton beam rate of $7.5 \times 10^9\,\text{s}^{-1}$ the secondary beam rate was $13 \times 10^6\,\text{s}^{-1}$, with an average difference between positive and negative rates of less than 5%. A simple trigger with large acceptance and single-bucket (18.9 ns) time resolution was used to select Ξ-candidate events. The "cascade" (CAS) trigger selected events with a $\Lambda \to p\pi$ topology by requiring at least one hit in each of the OS and SS hodoscopes (the "left-right" (LR) subtrigger) and at least 40 GeV of energy deposited in the hadronic calorimeter, an amount well below that deposited by the lowest energy p or $\overline{p}$.

The *CP* asymmetry $A_{\Xi\Lambda}$ was extracted by comparing the p and $\overline{p}$ $\cos\theta$ distributions in the Λ helicity frame. Special care was taken to exactly reverse the field of the Analyzing Magnets when switching modes, which kept the fractional difference between the magnitudes of the positive and negative fields to $\lesssim 3 \times 10^{-4}$ T. For these reasons biases due to spatial acceptance differences were minimal. Differences in the MWPC wire efficiencies were typically on the order of 1×10^{-3} in the secondary beam region and much

less outside. Hodoscope counter efficiency differences were usually small as well (10^{-3}). The calorimeter efficiency difference was $\approx 1 \times 10^{-3}$ and, within errors, uniform over the calorimeter face.

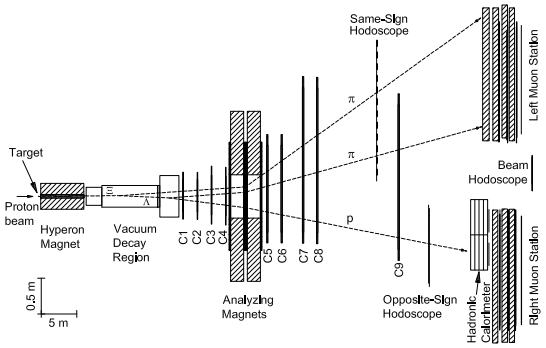

Figure 1. Plan view of the 1999 HyperCP spectrometer.

4. Analysis Technique

A total of 90×10^9 CAS triggers were recorded during the 1999 – 2000 production run. Tracks, particle momenta, invariant masses, and decay vertices were reconstructed using a $\Xi \rightarrow \Lambda\pi \rightarrow p\pi\pi$ hypothesis. Data were reduced to 2×10^9 Ξ^- and 0.5×10^9 Ξ^- and $\overline{\Xi}^+$ events respectively by requiring at least three final-state tracks and reconstructed Ξ and Λ masses within 50 MeV/c^2 of their PDG values [20].

Efficiencies of each MWPC wire and hodoscope counter were determined on a run-by-run basis using tracks from $\Xi^\pm$, $K^\pm$, and $\Omega^\pm$ events. These efficiencies were typically $\approx 99\%$ for the MWPCs and $> 99\%$ for the hodoscope counters. Calorimeter trigger efficiencies were measured on a run-by-run basis using LR subtrigger data and were usually higher than 99%. Runs with anomalously low ($\leq$ 95%) hodoscope, wire chamber, or calorimeter trigger efficiencies were not used. Likewise, runs which exhibited momentum- or position-dependent inefficiency differences with time-correlated opposite-polarity runs were also removed.

The criteria used to select the final event samples were: (1) that the $p\pi$ and $p\pi\pi$ invariant masses be within ± 5.6 MeV/c^2 (3.5σ) and ± 3.5 MeV/c^2 (3.5σ) respectively of the mean values of the Ξ and Λ masses (1.3220 and 1.1158 GeV/c^2); (2) that the z coordinate of the Ξ and Λ decay vertex lie within the vacuum decay region and that the Λ vertex precede the Ξ decay vertex by no more than 0.50 m; (3) that the reconstructed Ξ trajectory trace back to within ± 2.45 mm (3.3σ) and ± 3.26 mm (3.4σ) in x and y respectively of the center of the target; (4) that the Ξ trajectory trace back to within ± 10.5 mm and ± 6.5 mm, respectively, in x and y, from the center of the exit of the collimator; (5) that the $\pi^\pm\pi^\pm\pi^\mp$ invariant mass be greater than 0.5 GeV/c^2 (to remove $K \rightarrow \pi\pi\pi$ decays); and (6) that measured particle momenta fall in a kinematically allowed range given the constraints placed on the Ξ momentum by the Hyperon Magnet. Cuts were also made on the number of latched SS and OS hodoscope counters to ensure that the Ξ daughter-tracks fired (or could have fired) the trigger. Approximately 58.1% (44.7%) of the Ξ^- ($\overline{\Xi}^+$) events passed these selection requirements with an estimated background to signal ratio of approximately $(0.20 \pm 0.05)\%$ for both positive and negative data (Fig. 2).

The spectrometer was identical for both Ξ^- and $\overline{\Xi}^+$ decays; as such, the detector acceptance affected both the p and $\overline{p}\cos\theta$ distributions equally. However, production differences for Ξ^- and $\overline{\Xi}^+$'s led to different particle-antiparticle momentum distributions (Fig. 3) at the collimator exit. These differences in momentum can bias the p and $\overline{p}\cos\theta$ distributions with respect to each other. To correct for the production differences, events were weighted in five momentum-dependent variables and the ratio of the p and $\overline{p}\cos\theta$ distributions formed. The resultant ratio was fit to the form

$$R = C\frac{1 + \alpha_\Xi \alpha_\Lambda \cos\theta}{1 + (\alpha_\Xi \alpha_\Lambda - \delta)\cos\theta}, \qquad (6)$$

where the scale factor C is known from the sums

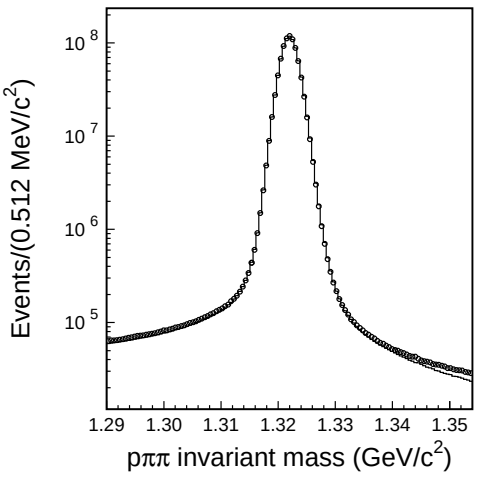

Figure 2. The $p\pi^-\pi^-$ (histogram) and $\overline{p}\pi^+\pi^+$ (circles) invariant masses.

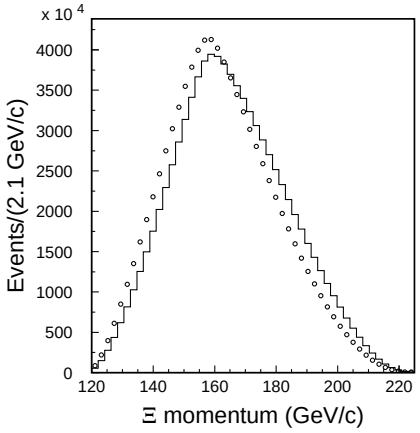

Figure 3. The Ξ^- (histogram) and $\overline{\Xi}^+$ (circles) momentum before weighting.

of the weights and $\delta = \alpha_\Xi\alpha_\Lambda - \overline{\alpha}_\Xi\overline{\alpha}_\Lambda$. The observable, $A_{\Xi\Lambda}$, was computed by substituting the PDG value of $\alpha_\Xi\alpha_\Lambda$ [20] and δ from the fit into Eq. 3 yielding

$$A_{\Xi\Lambda} \approx \frac{\delta}{2\alpha_\Xi\alpha_\Lambda}. \quad (7)$$

The weights were determined by binning five momentum-dependent parameters: the Ξ momentum magnitude p_Ξ, the Ξ y (y_Ξ) and x (x_Ξ) coordinates at the exit of the collimator, and the Ξ y (s_{Ξ_y}) and x (s_{Ξ_x}) slopes. The parameters p_Ξ, y_Ξ, and s_{Ξ_y} were each grouped into 50 bins, while 20 were used for the x_Ξ and s_{Ξ_x} distributions for a total of 50×10^6 bins. Fewer bins were used for the x position and slope because the bend plane of the Hyperon Magnet was in the y direction leading to larger differences in those distributions, and also because using too many leads to low average bin occupancy. Bins with fewer than four events of either polarity had their weights set to zero. Despite the relatively large number of bins compared to the size of the data sample, the average bin occupancy of bins with a nonzero weight was quite high, 795 Ξ^- and 274 $\overline{\Xi}^+$ events per bin. Table 1 lists the number of bins, the cell size, and the region over which each parameter was binned.

Table 1
Parameters used to define the bin weights.

Parameter	No. of Bins	Bin Size	
p_Ξ	50	2.10	GeV/c
y_Ξ	50	2.60	cm
s_{Ξ_y}	50	0.16	mrad
x_Ξ	20	1.05	cm
s_{Ξ_x}	20	0.20	mrad

Inefficiency differences were relatively small. However, due to the large number of events it was determined that the hodoscope efficiency differences had a significant effect on the result. To correct for the hodoscope inefficiencies, each event was first weighted; then the binning procedure

was applied to these weighted events. The hodoscope weight was calculated as the inverse of the hodoscope event efficiency, ϵ, given by

$$\epsilon = [1 - \prod_{\mathrm{OS}i}(1 - f_i)] \times [1 - \prod_{\mathrm{SS}i}(1 - f_i)], \qquad (8)$$

where the f_i are the efficiencies of the individual hodoscope counters. The products were preformed over each of the SS (SS_i) and OS (OS_i) counters hit by Ξ daughter particle tracks during the event. The average hodoscope weight was ≈ 1.005 and the magnitude of the correction on $A_{\Xi\Lambda}$ was 0.7×10^{-4}.

5. Monte Carlo Verification

The analysis algorithm was verified by a simulation called the collimator hybrid Monte Carlo (CHMC), which used momenta, positions, and slopes at the collimator exit from real Ξ^- and $\overline{\Xi}^+$ events as the seeds to computer generated Ξ decays. The simulation could be altered to produced *CP* asymmetries in both Ξ and Λ hyperon decays. To accurately ascertain the success of the algorithm, approximately 42×10^9 decays were generated. The analysis of such a large number of events was computationally demanding, so CHMC simulations were run on Fermilab's General Purpose Grid where a large amount of processing power was available. Application of the weighting algorithm required that events were first generated and binned; then a second process was run to calculate weights and compute the $\cos\theta$ distribution. This required that all generated data be written to an easily accessible scratch disk instead of slower tape-based systems. Scratch disk space was limited so the total output could not exceed 400 GB. To compensate, the data were segmented into subsets and each asymmetry was generated via twelve independent simulations. The CHMC subsets contained positive and negative runs which were correlated in time. A simulation of a null input asymmetry is illustrated in Fig. 4 along with the χ^2 per degree-of-freedom for each of the twelve fits.

The weighting technique was applied to generated data with input asymmetries (δ) of 0, 5×10^{-4}, -10×10^{-4}, 20×10^{-4}, and 50×10^{-4}.

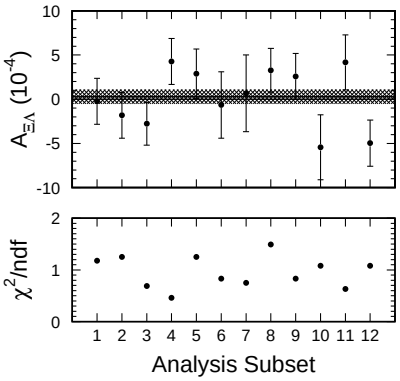

Figure 4. Measured asymmetry versus MC subset for zero input asymmetry and χ^2/dof values for each of the fits. The shaded area corresponds to the weighted average from the twelve data points. This figure corresponds one $A_{\Xi\Lambda(\mathrm{input})} = 0$ point on Fig. 5

Figure 5 shows that the technique recovers the input asymmetry with a small, but significant offset of $(-0.7 \pm 0.2) \times 10^{-4}$ (input minus measured) which was treated as a systematic error on the final result.

6. Preliminary Results and Systematic Errors

The ratio of the p and $\overline{p}$ $\cos\theta$ distribution from 863 million Ξ^- events and 230 million $\overline{\Xi}^+$ events is shown in Fig. 6. The fit to Eq. 6 yields a value, $\delta(base) = (3.1 \pm 1.3) \times 10^{-4}$, with a χ^2/dof of 1.2. This gives an asymmetry of $A_{\Xi\Lambda}(base) = (-5.3 \pm 2.1) \times 10^{-4}$, where the error is statistical.

The background-corrected asymmetry was determined by measuring the asymmetries of the mass sidebands 1.290 – 1.310 GeV/c^2 and 1.334 – 1.354 GeV/c^2 using the procedure outlined in Sec. 4 with the weights defined by events from the central region. The asymmetries from the two

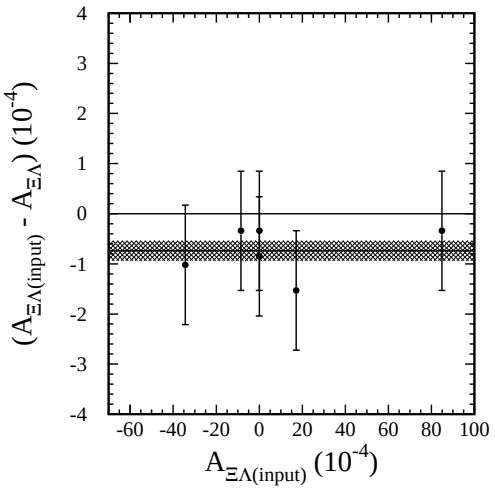

Figure 5. Asymmetry difference (input minus measured) versus the input asymmetry. The shaded area corresponds to the weighted average of the six measurements. The offset between the measured and input values is $(0.7 \pm 0.2) \times 10^{-4}$.

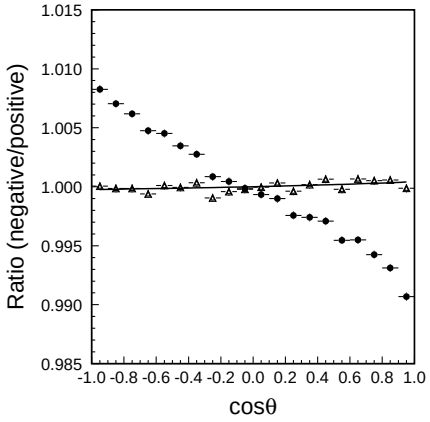

Figure 6. Preliminary ratios of p to $\overline{p}$ $\cos\theta$ distributions from the 1999 HyperCP dataset, both unweighted (circles) and weighted (triangles), with a fit to the weighted data of the form given in Eq. 6

sidebands were averaged, then scaled by the background fraction of 0.20% and subtracted from the base asymmetry to give $A_{\Xi\Lambda} = (-6.0 \pm 2.1) \times 10^{-4}$. The result was found to be stable with respect to time, Ξ momentum, and secondary beam intensity.

Differences in detector efficiencies between positive and negative running modes were generally small. Thus corrections were made only for the hodoscope efficiencies as outlined in Sec. 4. An upper limit was placed on the uncertainty in this correction by varying the hodoscope event efficiency by $\pm\sigma$ where σ is the propagated error from the errors calculated in the efficiencies of each hodoscope counter. When the event efficiency was increased by σ, the hodoscope event weight was bounded at one. The effect of the calorimeter inefficiency differences was estimated using the data sample collected with the LR trigger. The difference in $A_{\Xi\Lambda}$ with and without the calorimeter trigger requirement was found to be consistent with zero, with a statistical error of 0.9×10^{-4}. Effects from MWPC inefficiency differences (0.4×10^{-4}) were estimated using CHMC data by determining the difference in $A_{\Xi\Lambda}$ using real and 100% efficiencies. Table 2 lists the systematic errors. Added in quadrature, they give a overall systematic error of 2.0×10^{-4}.

Hall probes with a specified resolution of 0.5 Gauss were used to correct for the Analyzing Magnets field on a spill-by-spill basis. Errors in the Hall probe readings bias the result if they affect positive and negative data differently. The Hall probes were calibrated before the 1997 run and then later after the completion of the experiment in 2003. The initial calibration showed the two probes measured positive- and negative-polarity fields of equal magnitude to within 1 Gauss. The 2003 calibration revealed a bias of approximately 4 Gauss and 6 Gauss for the two Hall probes when comparing measurements of equal-magnitude opposite-polarity fields. Assuming

Table 2
Systematic uncertainty estimates (Preliminary)

Source	Error ($\times 10^{-4}$)
Calorimeter inefficiency	0.9
Earth's magnetic field	0.9
Spectrometer interactions	0.9
Analyzing Magnets' fields	0.7
Validation of analysis code	0.7
Hodoscope efficiency correction	0.4
MWPC inefficiency	0.4
Momentum bin size	0.4
Error on $\alpha_\Xi \alpha_\Lambda$	0.007
Background subtraction	0.003
Total	2.0

a linear degradation between the two calibrations, the bias at between measuring positive- and negative-polarity fields was approximately 3.5 Gauss during the 1999–2000 run. A simulation was performed in which a known field bias was inserted into the code used to reconstruct the Λ and $\overline{\Lambda}$ masses. By varying the field bias, it was determined that the difference between the mean Λ and $\overline{\Lambda}$ masses changes by $+3.80$ keV/c^2 per Gauss difference in the fields. Examination of the Λ and $\overline{\Lambda}$ masses revealed an average difference of 1.74 keV/c^2. In twelve time-correlated subsets of the data, the maximum difference between the Λ and $\overline{\Lambda}$ masses was 3.29 keV/c^2. These data suggested that the Hall probes functioned equally for positive and negative running to within 1 Gauss which leads to an uncertainty in $A_{\Xi\Lambda}$ of 0.7×10^{-4}.

The process used to verify the analysis algorithm was described in Sec. 5. Though Table 2 lists the measured offset of $(0.7 \pm 0.2) \times 10^{-4}$ as a systematic uncertainty, this could be corrected for by subtracting this quantity from the final result.

Also studied was the systematic effect of the bin sizes used to calculate the event weights. Because the p and $\overline{p}$ $\cos\theta$ distributions are most sensitive to momentum, this effect (0.4×10^{-4}) was estimated by varying the number of Ξ momentum bins by ±20% and taking the largest deviation in the final result as the estimate for the systematic uncertainty.

Also significant was the earth's magnetic field which causes spectrometer acceptance differences not accounted for by the weighting technique. This effect (0.9×10^{-4}) was estimated with the CHMC. Simulations were run with and without the earth's field to determine yielding a statistics-limited upper limit on the real error. Production differences between Ξ^- and $\overline{\Xi}^+$'s may facilitate a momentum-dependent differential loss of of events due to interactions within the spectrometer material. Using differential cross sections given in Ref. [20], an external Monte Carlo simulation was performed in which particles were allowed to interact within the spectrometer, from which an upper limit of 0.9×10^{-4} was placed on the size of this effect [18].

7. Conclusion

From 862×10^6 Ξ^- and 230×10^6 $\overline{\Xi}^+$ decays, we report a preliminary result result for the *CP* observable, $A_{\Xi\Lambda}$, to be $[-6.0 \pm 2.1(\text{stat}) \pm 2.0(\text{syst})] \times 10^{-4}$. This result is consistent with our previous result [18] and more than forty times as precise as the best result from other experiments [17]. Figure 7 shows the improvement in hyperon *CP* asymmetry measurements over time.

8. Acknowledgements

The authors would like to thank the organizers of BEACH 2008 for creating an educational and rewarding conference. Thanks also goes to the staffs of Fermilab and the participating institutions for their vital contributions. This work was supported by the U.S. Department of Energy. E.C.D and K.S.N were partially supported by the Institute for Nuclear and Particle Physics. K.B.L was partially supported by the Miller Institute.

REFERENCES

1. J. Christenson *et al.*, Phys. Rev. Lett. **13**, 138 (1964); A. Alavi-Harati, *et al.*, Phys. Rev. Lett. **83**, 22 (1999); V. Fanti *et al.*, Phys. Lett. B **465**, 335 (1999).

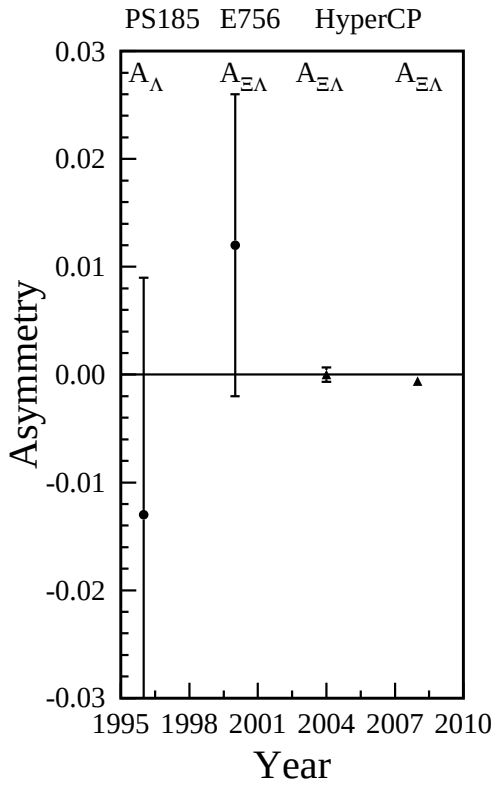

Figure 7. *CP* asymmetry measurements in Ξ and Λ hyperon decays from PS185 [21], E756, and HyperCP.

2. A.D. Sakharov, Pis'ma Zh. Eksp. Teor. Fiz 5, 32-35 1967; JETP Lett. **5**, 24-27 (1976).
3. M. Kobayashi and T. Maskawa, Prog. Theor. Phys. **49**, 652 (1973).
4. A.G. Cohen, D.B. Kaplan, and A.E. Nelson, Annu. Rev. Nucl. Part. Sci. **43**, 27 (1993).
5. B. Aubert *et al.*, Phys. Rev. Lett. **87**, 091802 (2001); K. Abe *et al.*, Phys. Rev. Lett. **87**, 091802 (2001); Y. Chao *et al.*, Phys. Rev. Lett. **93**, 191802 (2004); B. Aubert *et al.*, Phys. Rev. Lett. **93**, 191802 (2004).
6. The Belle Collaboration, Nature **452**, 332 (2008).
7. N.G. Deshpande, X.-G. He, and S. Pakvasa, Phys. Lett. B **326**, 387 (1994).
8. J. Tandean, Phys. Rev. **69**, 076008 (2004).
9. A. Pais, Phys. Rev. Lett. **3**, 242 (1959).
10. T.D. Lee and C.N. Yang, Phys. Rev. **108**, 1645 (1957).
11. J.F. Donoghue and S. Pakvasa, Phys. Rev. Lett. **55**, 162 (1985); J.F. Donoghue, X.-G. He, and S. Pakvasa, Phys. Rev. D **34**, 833 (1986); D. Chang, X.-G. He, and S. Pakvasa, Phys. Rev. Lett. **74**, 3927 (1995).
12. J. Tandean and G. Valencia, Phys. Rev. D **67** 056001 (2003).
13. J. Tandean, A.W. Pakvasa, and G. Valencia, Phys. Rev. D **64**, 014005 (2001).
14. M. Huang *et al.*, Phys. Rev. Lett. **93** 011802 (2004); A. Chakravorty *et al.*, Phys. Rev. Lett. **91**, 031601 (2003).
15. X.-G. He, H. Murayama, S. Pakvasa, and G. Valencia, Phys. Rev. D **61**, 071701(R) (2000).
16. C.-H. Chen, Phys. Lett. B **521**, 315 (2001).
17. K.B. Luk *et al.*, Phys. Rev. Lett. **85**, 4860 (2000).
18. T. Holmstrom *et al.*, Phys. Rev. Lett. **93** 262001 (2004).
19. R.A. Burnstein *et al.*, Nucl. Instrum. Meth. A **541**, 516 (2005).
20. W.-M. Yao *et al.*, J. Phys. G: Nucl. Part. Phys. **33**, 1067 (2006).
21. P.D. Barnes *et al.*, Phys. Lett. B **199**, 147 (1987).; P.D. Barnes *et al.*, Phys. Rev. C **54**, 1877 (1996).